

Overview of Past Projects Portfolio

Xing-Yu Chen, M. Sc.

October 13, 2023

1 Continuum Surgical Robot

Continuum robot has evolved as a novel treatment modality with better features over the traditional minimally invasive surgery, such as faster, safer, and more convenient intra-body interventions without wide incisions. They are designed to navigate anatomical pathways through single-port access, e.g. natural orifice transluminal endoscopic surgery or minimal incisions. Continuum surgical robots have a fundamentally different structure than conventional manipulators composed of discrete rigid links connected by joints. Their ability to take the shape of 3D curves enables these robots to perform procedures through smaller surgical corridors than would be possible with traditional robotic mechanisms. During the work in Shenzhen Institute of Advanced Technology, Chinese Academy of Sciences, I lead a small group of students and design two continuum robot, a vascular interventional surgical robot and a robotic bronchoscopy system.

1.1 Novel Robotic Bronchoscopy System

Related Publication:

Chen, Xing-Yu, et al. *Design of a Teleoperated Robotic Bronchoscopy System for Peripheral Pulmonary Lesion Biopsy*. arXiv preprint arXiv:2306.09598(2023).

CN Patent: *A sheath with continuously adjustable stiffness, its stiffness adjustment method, and surgical equipment*. CN115920200A.

CN Patent: *Biopsy Forceps Storage and Delivery Device for Bronchoscope Surgical Robots*. CN115429343A.

CN Patent: *A Respiratory Diagnosis and Treatment Robot System and its Control Method*. PCT/CN115252146.

CN Patent: *A bronchoscope module and its biopsy method*. CN116369834A.

I am currently tasked with designing an innovative teleoperated robotic bronchoscopy system and multi-modal navigation through image and electromagnetic sensors. During the procedure, the surgeon holds a tablet console to control a flexible visual bronchoscope, inserts a flexible tube into the patient's mouth, and utilizes the robot for advancements, rotations, and adjustment of the bending angle of the front end of the flexible

bronchoscope. The robot also enables control of the biopsy forceps for feeding and tissue sampling.

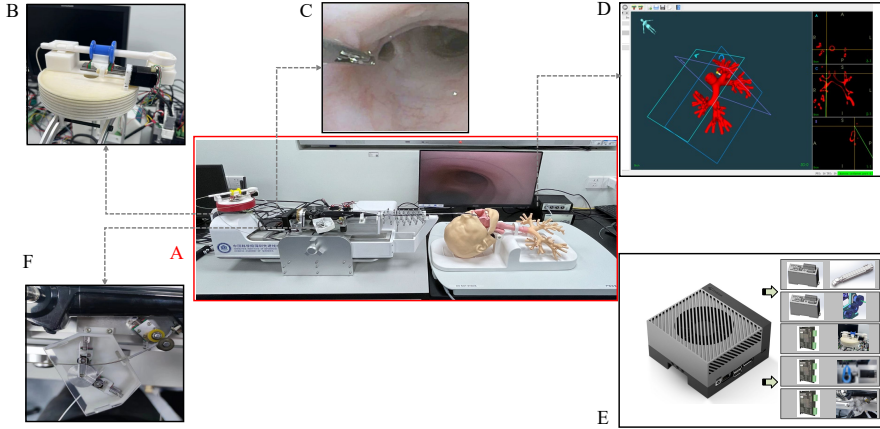


Figure 1: Robotic Bronchoscopy System. (A) Robot and bronchus phantom; (B) Biopsy forceps manipulator; (C) Bronchoscopic video. (D) EM-Sensor based navigation system; (E) Embedded control system, electrical devices and motors; (F) Biopsy forceps and Catheters delivery device.

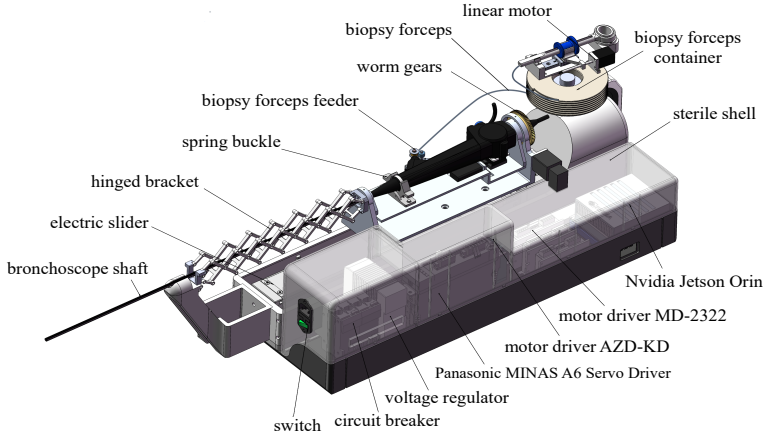


Figure 2: Structure of the bronchoscope robot.

The system consists of a teleoperated surgical robot designed for trans-respiratory diagnosis, along with a corresponding master-slave control system. It incorporates various components, including a flexible bronchoscope, bronchial biopsy instruments, variable stiffness catheters, a magnetic navigation device, and several tablets functioning as master consoles. The surgeon operates the tablet, and the instructions are wirelessly transmitted to the embedded system controller through the TCP/IP protocol suite. Subsequently, the robot manipulates the flexible bronchoscope in response to the is-

sued commands. Employing a multi-operator strategy, the robot is controlled through scheduling arrangement and weight distribution, which enables mentor surgeons and trainee surgeons operate surgery simultaneously. They can observe the same surgical site and share control of robotically controlled surgical instruments. This allows trainees to gain firsthand experience of the procedure while being guided by the mentor surgeon. Additionally, the mentor surgeon can switch control to selected trainees if necessary and override their control during the bronchoscopy procedure. I developed the electrical system of the entire surgical robot, and used pyqt to design the UI interface of the system, as shown in Fig.4. We have also developed a novel Variable Stiffness Catheter (VS-Catheter) composed of Low Melting Point Alloy (LMPA) to enhance the catheter's flexibility in the context of minimally invasive surgery and expand the accessible area for bronchoscopic biopsy forceps. Compared with bronchoscope, the VS-Catheter can be inserted into narrower bronchi and offers more flexible control with dynamic stiffness.

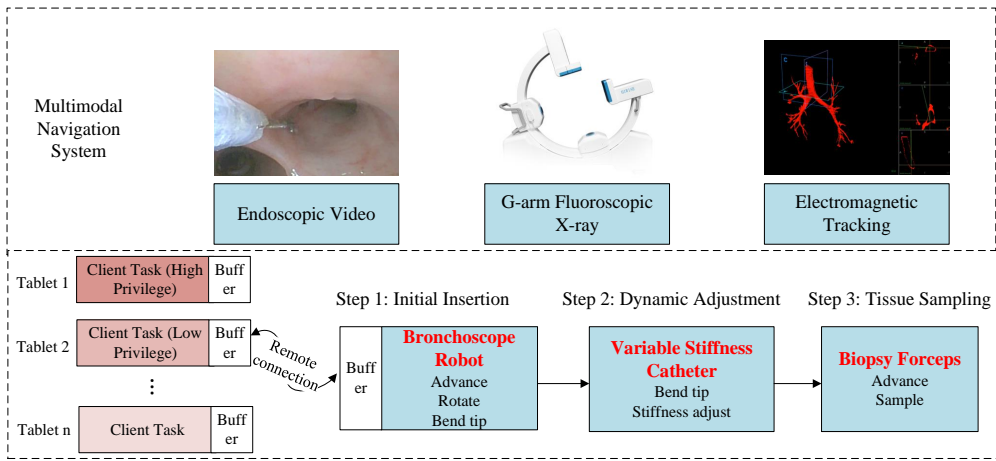


Figure 3: Proposed three-stage bronchoscopy surgical procedures, with initial insertion, dynamic adjustment, and tissue sampling.

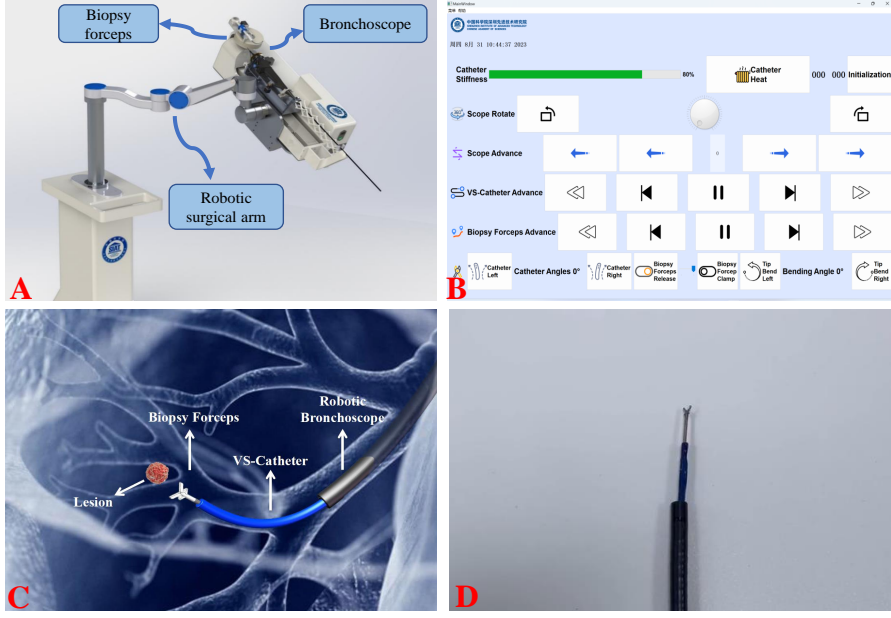


Figure 4: (A) Proposed robotic bronchoscopy system. (B) UI developed with PyQt. (C) Novel three-stage bronchoscopy surgical procedure composed of robotic bronchoscope, VS-Catheter, and tissue sampling by biopsy forceps. (D) The three-stage bronchoscopy surgical tools.

Additionally, to integrate endoscopic video and EM tracking information, I am employing a multimodal navigation system, utilizing the open-source software 3D Slicer, shown in Fig.5. It offers a range of tools for importing, processing, visualizing, and analyzing medical image data. It also provides capabilities for image registration, segmentation, and fusion. Furthermore, it includes a toolbox of navigation features, image-processing algorithms, and connections to external hardware for image-guided therapy (IGT). By combining images, tracked surgical instruments, and computer display, a comprehensive navigation system is created, enabling real-time identification of the direction and position of the bronchoscope tip and reference.

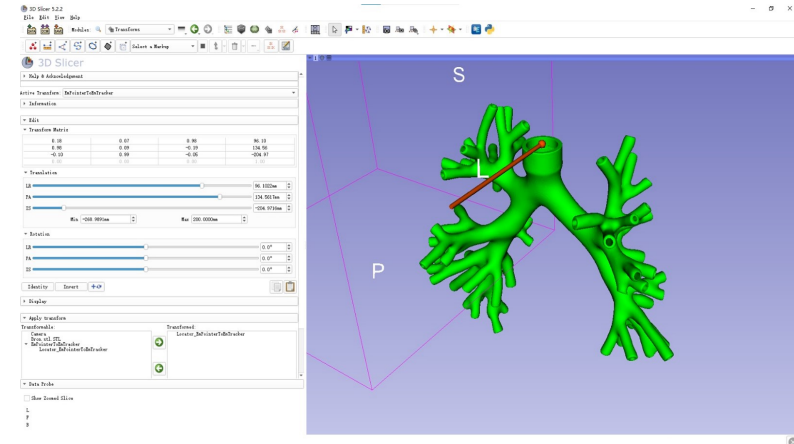


Figure 5: 3D Slicer and coordinate transform.

Fig.6 showed the surgery procedure of robot-assisted bronchoscopy. Registration involves creating a 3D map of the patient’s airways, integrated through CT or MRI to provide visual map of the surgical workspace. This map is used to guide the robotic system during the procedure. Once the registration is complete, the physician will use the 3D map to plan the bronchoscopy procedure. This may involve identifying the location of suspicious areas, such as tumors or lesions, and planning the best route to reach them. After the robotic system is set up on a passive arm and calibrated, the physician remotely controls the robotic system to examine the patient’s airways with virtual bronchial navigation or EM guidance navigation system, looks for any abnormalities or suspicious areas, and performs a biopsy or other procedure to obtain a tissue sample for further testing.

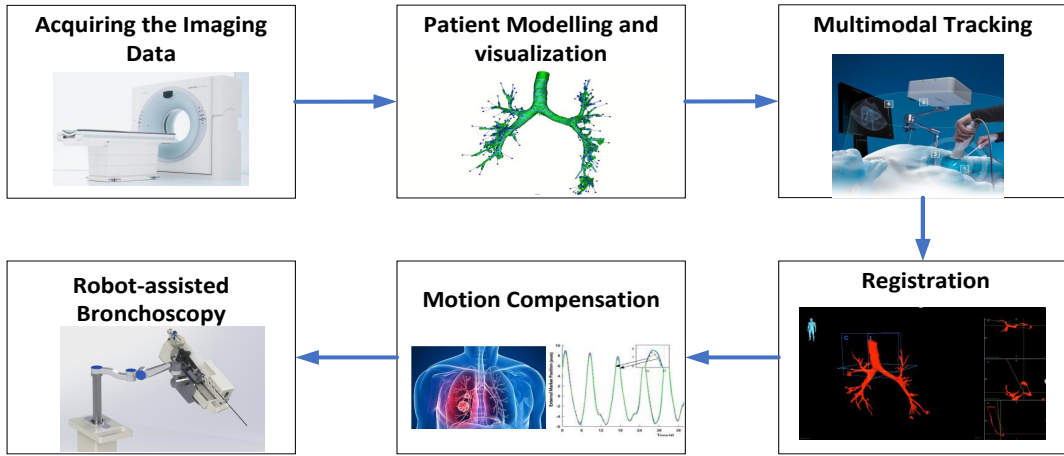


Figure 6: Robotic assisted bronchoscopy procedure.



Figure 7: Proposed bronchoscopy system. (A) In-vivo experiment; (B) The three-stage bronchoscopy tools in pig's trachea.

In addition, we conducted several animal biopsy experiments using the robotic bronchoscopy system, as depicted in Fig.7. The system was controlled by two operators using tablets with different priorities and EM sensors were attached to the pig's forebreast and the tip of the bronchoscope. We successfully performed a biopsy procedure in which small tissue was clamped and removed from the tertiary bronchus of a pig. The implementation of the VS-Catheter enabled more flexible control of the biopsy forceps within the bronchus. The stiffness of the catheter was adjusted by energizing the resistance wire, providing adaptability based on the specific requirements of the procedure. The usability and effectiveness of the designed bronchoscopy surgical robot were demonstrated. Our work has been submitted to the 2023 IEEE BioCAS conference for publication.

1.2 Vascular Interventional Surgical Robot

Related publication:

Chen, Xing-Yu, et al. *Design and Evaluation of a Learning-based Vascular Interventional Surgery Robot*. *Fibers*, 10.12 (2022): 106.

Akinyemi, T.O., et al. *Adapting Neural-Based Models for Position Error Compensation in Robotic Catheter Systems*. *Applied Sciences*, 12.21 (2022): 10936.

Akinyemi, T.O., et al. *Interventionalist Hand Motion Recognition with Convolutional Neural Network in Robot-assisted Coronary Interventions*. *IEEE Sensors Journal*.

Duan, Wenke, et al. *Technical and Clinical Progress on Robot-Assisted Endovascular Interventions: A Review*. *Micromachines*, 14.1 (2023): 197.

CN Patent: *A Tactile-Feedback Device and Method for Surgical Robots*. CN115137483A.

CN Patent: *A Bidirectional Guidewire Force Measurement Method for Vascular Interventional Surgical Robot*. CN114948258A.

I have designed an isomorphic master-slave Vascular Interventional Surgical Robot (VISR) for precise force measurement and navigation of endovascular tools viz. catheters and guidewires, as shown in Fig.8-10. The master console aids operators in issuing manipulation commands and logs feedback from the force, rotation, and translation data. The slave manipulator uses the commands received from the master platform for

actual tool navigation. Some force sensors are mounted at clamping device of the robot manipulator, so I utilized an Artificial Neural Network (ANN) for guidewire resistance force modulation with 50 mN precision. The developed ANN is a multilayer perceptron with five hidden layers and 77 neurons. The network is used to estimate distal force of guidewire from the force measured from force sensor in robot manipulator.



Figure 8: Vascular interventional surgical robot designed in SIAT, Chinese Academy of Sciences; (A) Master console; (B) Slave manipulator; (C) Surgeons teleoperate the master console in the room without being exposed to X-rays; (D) Slave manipulator placed next to pig in DSA room.

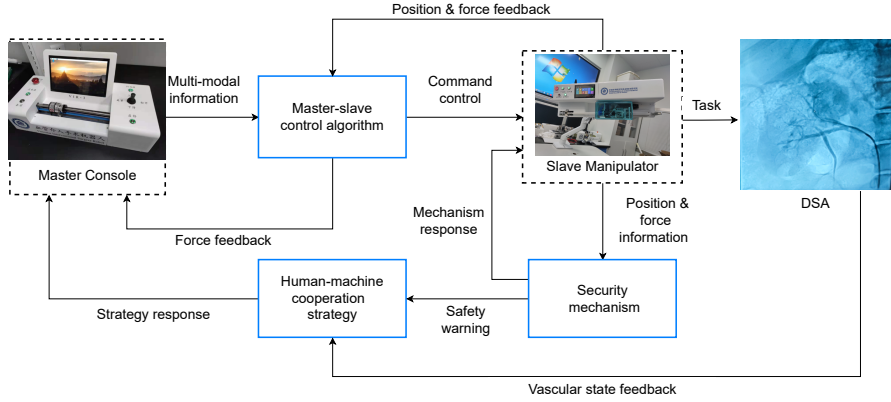


Figure 9: Control flow of the VISR. Surgeons teleoperate the doctor's terminal in the room without X-rays, and the slave manipulator with a robotic arm is placed beside the patient's bed.

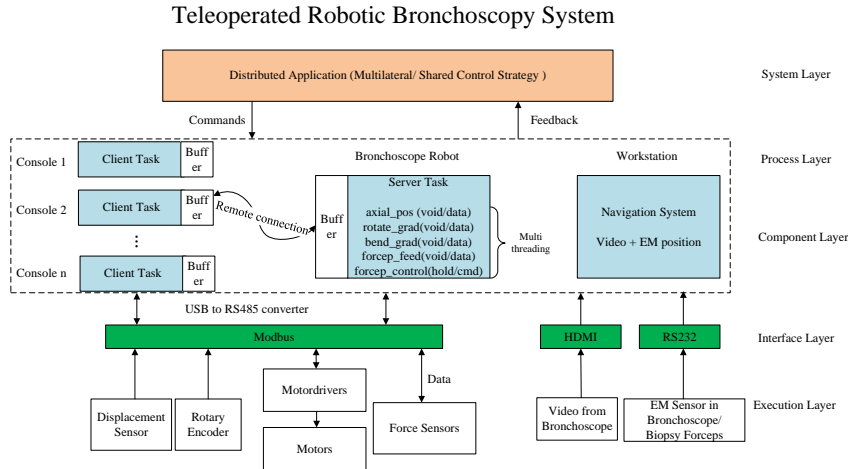


Figure 10: Layers of the VISR control architecture.

As shown in Fig.11, the robotic system includes a force box used for measuring the tactile force that interventionalists exerted with their fingers. This force is regarded as the interventionalists' operative force on the guidewire or catheter in regular surgery. The force box includes a 32-prism, tiny flexible strip sensors, PCBs, and batteries. A flexible sensor is folded and wound around the force box surface, and its data is logged as a 32-channel data multiplexed over an Analog Multiplexer (Texas Instruments). Thus, the interventionalists also operate the master device by manipulating the flexible sensor with their finger. The force data is processed in a microcontroller STM32 and transmitted over a Bluetooth module to the slave console in real time. The force box also reflects information about the flexible tool's firmness as it is held with a clamping mechanism in

the slave manipulator. The guidewire is clamped tightly when the surgeon presses hard on the force box and vice versa.

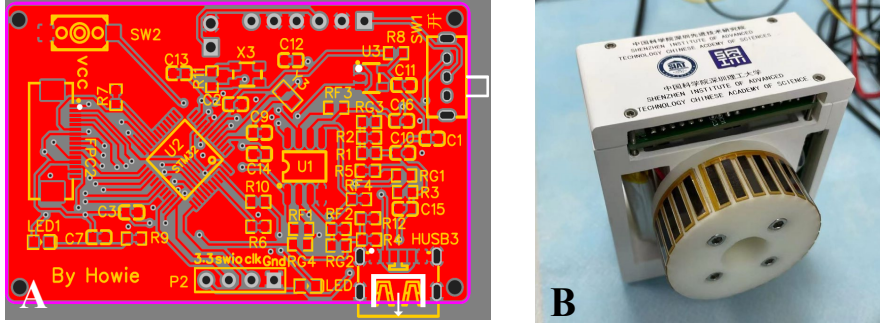


Figure 11: The structure of the force box, which can measure the tactile force exerted by the surgeon’s fingers. The force value will be used as parts of multi-modal information to optimize the control algorithm. (A) PCB layout of force box; (B) Force box includes a 32-prism, tiny flexible strip sensors.

To study the usage of robotic-assisted vascular interventions by surgeons and aid them in acquiring skills more efficiently, I designed a smart glove shown in Fig.12. This glove is capable of capturing and fusing information from multiple modalities, including the bending of the surgeon’s fingers, the forces exerted while manipulating the vascular surgical robot, electromyographic (EMG) signals, posture angles and accelerations (IMU), as well as spatial position and orientation collected using electromagnetic sensors.

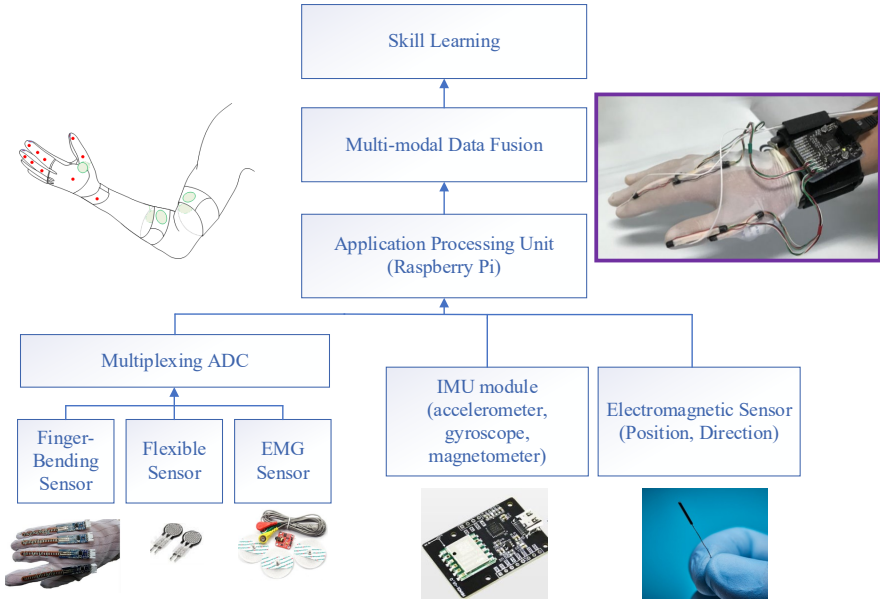


Figure 12: Intelligent glove for robotic catheterization skill learning.

In addition, I utilized fuzzy PID and recurrent neural network (RNN) models such as the Long Short-Term Memory networks (LSTM) and Gated Recurrent Unit (GRU) networks to learn typical motion dynamics when running the master-slave platform. The trained network could estimate the position of the slave robot based on input motion factors. The estimated value and an appropriate compensatory value are then transferred to the slave robotic device in order to map the master platform's movements uniformly. The RNN models were implemented in Python and using the Keras library and the TensorFlow framework. The LSTM model contains an input layer ($N \times 3 \times 3$), two hidden layer with 32 units each, and a fully connected layer that outputs a predicted value using the rectified linear unit (ReLU) activation function. The LSTM unit may extract essential features from an input sequence and store them in memory. To train the model, experimental data for various step values was stacked together, and feature scaling was applied to the data.

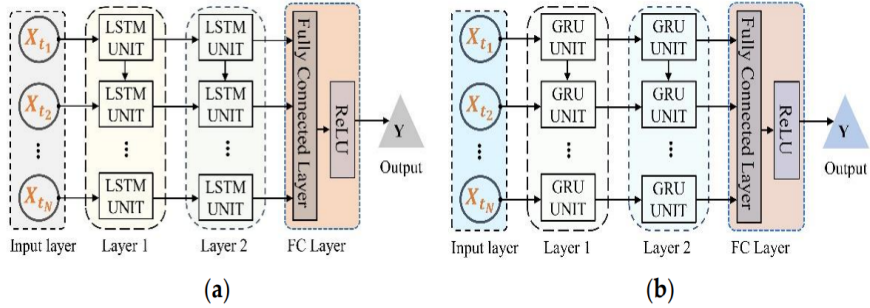


Figure 13: A stacked 2-layer architecture for robot position prediction and compensation using (a) LSTM and (b) GRU model.

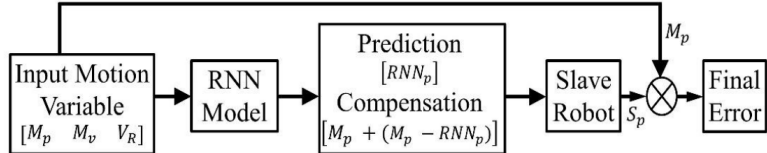


Figure 14: Control block with error compensation for the patient-side robot.

Fig.13 depicts the in-silico evaluations of the GRU and LSTM-based controllers. Although the original error increased to 40%(2.0mm) of the input command for several phases, the minimum and greatest final errors were 0.001 mm and 0.1mm (2% of the input command) across the steps. It depicts how the GRU-based controller may estimate the predicted slave robot response ahead of time and then use this to regress the initial position error. To validate the real-time usability of the learning-based models in the VISR, we utilized the Jetson AGX Orin development kit (NVIDIA, CA, USA) for the patient-side robot, and evaluated the model's performance under uniform and

varying input commands using the control block diagram presented in Fig.14. For a typical master's displacement, velocity, and the velocity ratio, the RNN model makes an appropriate prediction and checks for errors.

2 Driver Board of 4D Ultrasound

The 4D imaging in sonography is an advanced technique that enables real-time 3D ultrasound imaging of the fetus within the body, incorporating the element of time or motion. This technique is commonly employed in obstetrics to assess fetal growth, development, and identify any potential abnormalities or malformations. Furthermore, it finds application in various medical contexts, such as visualizing the heart or blood vessels in real-time. The introduction of 4D imaging has revolutionized prenatal imaging, granting expectant parents the opportunity to observe detailed, dynamic images of their developing baby in the womb.

During my previous work at Esaote, one of the world's leading ultrasound manufacturers, I actively contributed to the design of a novel ultrasound scanner system, as depicted in Fig.15. This experience provided me with a comprehensive understanding of the underlying principles and implementation methods of ultrasonography. The TMC5130A (Trinamic, Hamburg, Germany) served as a high-voltage general-purpose controller for two-phase bipolar stepping motors. Notably, this chip featured a serial communication interface, enabling automated target positioning. When paired with an external power transistor, it facilitated high dynamic range and high torque motor control.

The central function of the 4D driver board's CPU was to receive data from the host motherboard and issue various motor control instructions to the TMC5130A. To fulfill this role, I utilized the STM32F3 series chip, a 32-bit MCU based on ARM's Cortex-M4 core. With a voltage supply range of 2.0 to 3.6V, this microcontroller boasted 16k bytes of SRAM, two SPI interfaces, one ADC, and three USARTs. It supported crystal oscillators ranging from 4 to 32MHz and offered debugging capabilities via SWD or JTAG, effectively catering to the requirements of the 4D driver board's main control chip. The communication between the motor driver TMC5130A and the microcontroller STM32 was established using the SPI protocol.

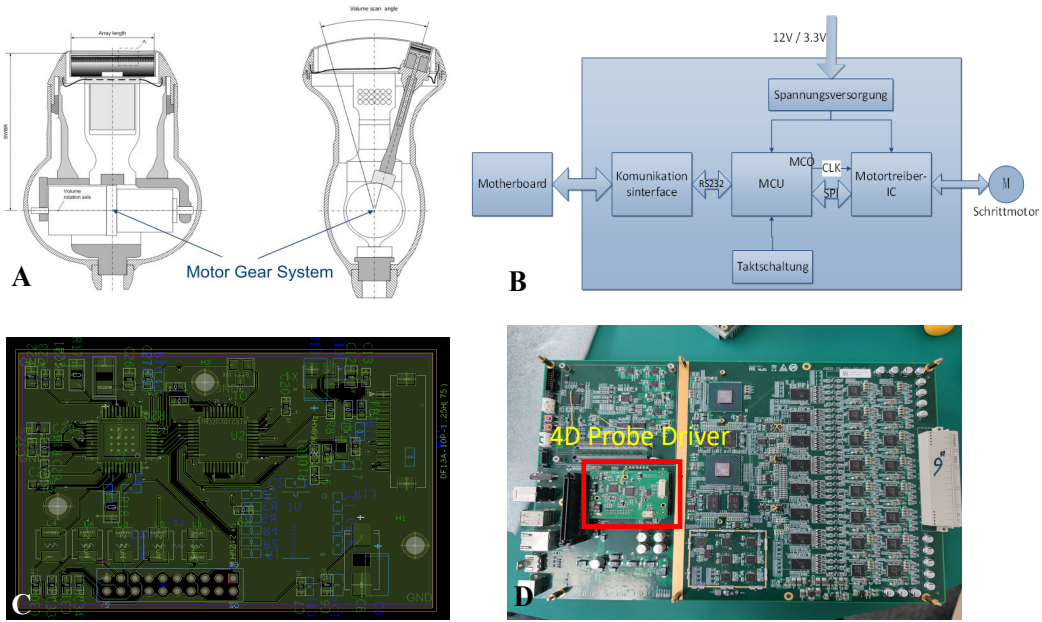


Figure 15: 4D probe system. (A) Structure of 4D probe; (B) 4D probe driver; (C) PCB layouts; (D) 4D probe driver in the ultrasound system, the PCB is inserted into the motherboard.

To mitigate the interference caused by the drive signal from the motor driver in the 4D-Probe, which affected the received signal from the ultrasonic transducer and introduced noise in the 4D imaging, I undertook several optimization measures. Firstly, I focused on optimizing the PCB layout of the motor driver within the 4D-Probe. By carefully arranging the components and traces, I aimed to minimize signal coupling and electromagnetic interference. Furthermore, I implemented shielding covers to establish spatial isolation for the motor driver. These covers acted as a barrier, preventing the drive signal from directly affecting the sensitive components and circuitry involved in receiving the ultrasonic signals. This shielding approach effectively reduced unwanted noise and interference. In addition, I incorporated layered ground structures into the design to counteract any interference stemming from ground currents. This involved creating separate ground planes and carefully managing the routing of ground connections, which aided in minimizing signal crosstalk and further enhancing the overall performance of the ultrasound imaging system. By implementing these optimization techniques, I successfully addressed the issue of signal interference and crosstalk, leading to improved image quality and enhanced signal integrity in the 4D imaging process, as shown in Fig.16.

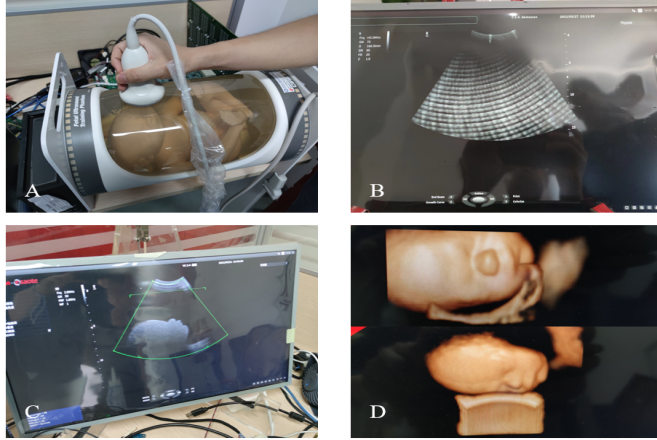


Figure 16: 4D imaging in sonography. (A) Fetal ultrasound training phantom; (B) Noise in the 4D imaging system; (C) Signal crosstalk eliminated; (D) Reconstructed fetus model.

3 Magnetic Nanoparticle Imaging Scanner

As an emerging tomographic imaging modality, Magnetic Particle Imaging (MPI) has many potential uses in biomedical engineering. It measures the magnetization response of superparamagnetic iron oxide nanoparticles and images the spatial distribution of tracer material. Unlike other tomographic imaging techniques, such as Positron Emission Tomography (PET) and Single Photon Emission Computed Tomography (SPECT), MPI is entirely free of ionizing radiation, which benefits the safety of patients and medical staff. The main challenge faced by many researchers is the detection sensitivity of the MPI scanner and the high signal-to-noise ratio (SNR) requirements in the MPI system. The amplitude of the signal, which is detected by the receive coil, could be extremely low. In this situation, the signal must be amplified with a low-noise amplifier (LNA). In master's thesis at TU Braunschweig, I focused on analyzing the noise characteristics of the MPI receive system and proposed two methods to improve the noise performance over a wide-band frequency range: a ferrite core transformer and a LNA. The prototype LNA consisted of four parallel amplifiers and a summing circuit, resulting in a significant improvement in the noise performance of the MPI receive chain.

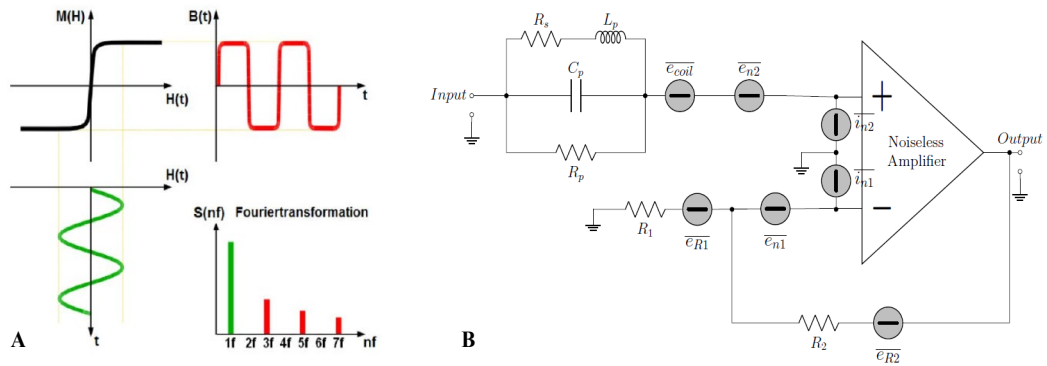


Figure 17: Principle of Magnetic Particle Imaging. (A) The relationship between the external magnetic field and the magnetization of magnetic nanoparticles. (B) Noise model of the MPI scanner receive chain.

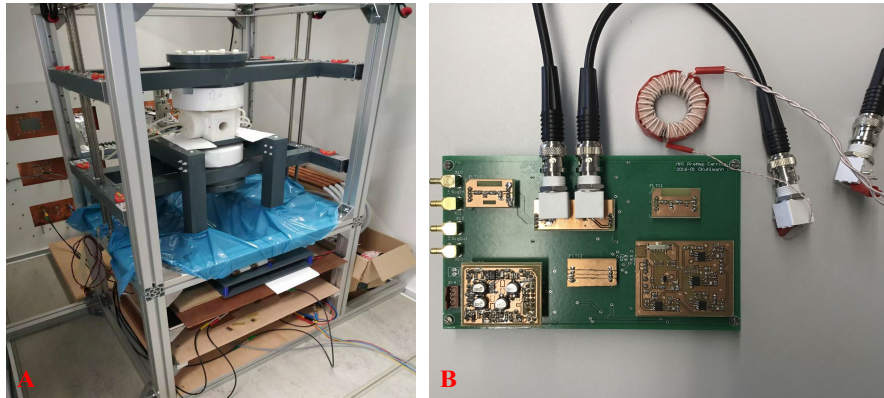


Figure 18: Magnetic Particle Imaging system in TU Braunschweig, Germany. (A) MPI scanner. (B) Proposed LNA and ferrite core transformer.